TITLE PAGE

Upregulation of the lactate transporter monocarboxylate transporter 1 at the blood-brain barrier in a rat model of attention-deficit/hyperactivity disorder suggests hyperactivity could be a form of self-treatment

Tirill Medin[1,2,3*], Hege Medin[4], Marita Brandsar Hefte[3], Jon Storm-Mathisen[3] and Linda Hildegard Bergersen[2,3,5]

[1]OsloMet - Oslo Metropolitan University, Faculty of Health Sciences, P.O. Box 4, St. Olavs Plass, 0130 Oslo, Norway.

[2]The Brain and Muscle Energy Group, Electron Microscopy Laboratory, Department of Oral Biology, University of Oslo, NO-0316 Oslo, Norway.

[3]Synaptic Neurochemistry and Amino Acid Transporters Labs, Division of Anatomy, Department of Molecular Medicine, Institute of Basic Medical Sciences (IMB) and Healthy Brain Ageing Centre (SERTA), University of Oslo, NO-0317 Oslo, Norway.

[4]Norwegian Institute of International Affairs (NUPI), Pb 8159 Dep, 0033 Oslo, Norway.

[5]Center for Healthy Aging, Department of Neuroscience and Pharmacology, Faculty of Health Sciences, University of Copenhagen, DK-2200 Copenhagen N, Denmark.

© 2018. This manuscript version is made available under the CC-BY-NC-ND 4.0 license
http://creativecommons.org/licenses/by-nc-nd/4.0/

*Correspondence to:

Tirill Medin, OsloMet - Oslo Metropolitan University, Faculty of Health Sciences, P.O. Box 4, St. Olavs Plass, 0130 Oslo, Norway. E-mail: tirill.medin@oslomet.no

Declaration of interest:

None

Abbreviations:

ADHD, attention-deficit/hyperactivity disorder; ADHD-C, combined subtype of ADHD; BBB, blood-brain barrier; MCT, monocarboxylate transporter; PND, postnatal day; SHR, spontaneously hypertensive rat; SHR/NCrl, SHR from Charles River, Germany; WKY, Wistar Kyoto rat; WKY/NHsd, WKY from Harlan Europe, UK

© 2018. This manuscript version is made available under the CC-BY-NC-ND 4.0 license
http://creativecommons.org/licenses/by-nc-nd/4.0/

ABSTRACT

The energy deficit hypothesis of attention-deficit/hyperactivity disorder (ADHD) suggests that low lactate production by brain astrocytes causes the symptoms of the disorder. Astrocytes are the main producers of lactate in the brain; however, skeletal muscles can produce the most lactate in the body. The lactate production by skeletal muscles increases with physical activity, as does the expression of the lactate transporter monocarboxylate transporter 1 (MCT1) at the blood-brain barrier (BBB). We hypothesise that children with ADHD, by being hyperactive, increase lactate production by skeletal muscles and transport it into the brain to compensate for low supply by astrocytes. The aim of this study was to explore whether the level of MCT1 is altered in the brain in an animal model of ADHD. The MCT1 expression was quantified on hippocampal brain sections from the best available rat model of ADHD, i.e., the spontaneously hypertensive rat (SHR) (n=12), and the relevant control, the Wistar Kyoto rat (WKY) (n=12), by the use of quantitative immunofluorescence laser scanning microscopy and postembedding immunogold electron microscopy. The results revealed significantly higher levels of hippocampal MCT1 immunoreactivity in SHR compared to WKY, particularly at the BBB. These results indicate that lactate flux through MCT1 between the body and the brain could be upregulated in children with ADHD. This study adds to previous research suggesting hyperactivity may be beneficial in ADHD; Children with ADHD possibly display a hyperactive behaviour in order to raise skeletal muscle lactate production, MCT1 expression and flux over the BBB to supply the brain with lactate.

Keywords: Electron microscopy; hippocampus; immunofluorescence; postembedding immunogold quantification; spontaneously hypertensive rat

© 2018. This manuscript version is made available under the CC-BY-NC-ND 4.0 license
http://creativecommons.org/licenses/by-nc-nd/4.0/

1. INTRODUCTION

Attention-deficit/hyperactivity disorder (ADHD) is a common psychiatric condition [1] recognized by three main symptoms: inattention and/or hyperactivity and impulsivity [2]. Children with combined symptoms of the disorder (ADHD-C), struggle with both impaired attention and a hyperactive-impulsive behaviour [2]. The cause of ADHD is debated [3, 4]. Some hypotheses of ADHD claim the symptoms result from an energy deficit in the brain [5-7]. The brain requires around 20 % of the total energy supply in the body at physical rest [8]. The high energy consumption is mainly due to the cost of restoring postsynaptic cell resting membrane potential after activation [8]. The brain primarily consumes glucose in order to produce ATP, but in addition, lactate serves as a fuel for neurons [9, 10]. Lactate produced by astrocytes in the brain [11] can be shuttled into activated neurons [12], and be essential for processes such as memory formation [13]. Todd and Botteron (2001) hypothesized that ADHD may result from low lactate availability for neurons, as a consequence of hypofunctional catecholamine stimulation responsible for increasing lactate production in astrocytes [7]. Russell et al. (2006) further suggested that deficient lactate supply by astrocytes could result in reduced energy availability for neurons and for myelination of axons, leading to abnormal behaviour observed in children with ADHD [6]. Defects in enzymes, receptors or transporters affecting the astrocyte-neuron-lactate-shuttle may result in ADHD symptoms [5, 14].

Lactate cannot freely cross cell plasma membranes, but is dependent on specific transporters of the monocarboxylate transporter (MCT) family [15]. The lactate transport is coupled to

© 2018. This manuscript version is made available under the CC-BY-NC-ND 4.0 license
http://creativecommons.org/licenses/by-nc-nd/4.0/

proton transport and the direction of flux depends on the lactate and proton gradients. MCT1, MCT2 and MCT4 are present in the brain. In rodents, neurons primarily express MCT1 [16] and MCT2 [17], whereas astrocytes express MCT1 [17] and MCT4 [18]. Lactate produced by astrocytes through the metabolic breakdown of glucose may exit the astrocyte by MCT1 and MCT4 for further utilization by neurons [19]. However, MCT1 is especially abundant at the blood-brain barrier (BBB), comprising endothelial cells of cerebral capillaries [18, 20], thus MCT1 is the MCT that can transport peripheral circulating lactate into the brain. Despite the fact that skeletal muscle is the main producer of lactate in the body, and hyperactivity is a main feature of ADHD, no emphasis has previously been made to explore the potential role of MCT1 in the brain in ADHD.

Dysfunctions in prefrontal cortex have been linked to inattention in ADHD [21], whereas disturbances in striatum, cerebellum and motor cortex have been associated with hyperactivity [22]. A recent review suggests that abnormalities in hippocampus are important to several psychiatric disorders including ADHD, as hippocampus is part of a multiple memory system [23]. Hippocampus has a main function in learning, being important to both short term [24] and long term memory [25]. Learning disabilities have been observed in studies of ADHD symptomatology [14, 26, 27] and abnormalities in hippocampus may be associated with ADHD symptoms [28]. More specifically, recent research shows that hippocampal volumes are reduced in the subtype ADHD-C, whereas the volumes are normal in the inattentive subtype [29]. The hippocampus has a unique role in the brain as a region in which neurogenesis occurs throughout life. The hippocampus has a particularly high density of MCT1 compared to several other brain regions [30] and lactate entering the brain through these transporters may affect brain plasticity through both functional and structural changes.

© 2018. This manuscript version is made available under the CC-BY-NC-ND 4.0 license
http://creativecommons.org/licenses/by-nc-nd/4.0/

During the last decade, the use of animal models of ADHD has revealed alterations in transmitters and receptors involved in neuronal signaling in hippocampus [31-34]. Hence, the hippocampus is a brain region of interest to explore ADHD aetiology.

Some models of ADHD suggest that hyperactivity has a positive effect on cognitive functions [35, 36]. We hypothesize that children with ADHD are hyperactive to compensate for low lactate within the brain; physical activity is followed by elevated lactate production by skeletal muscle and enhanced MCT1 expression at the BBB, so that the lactate flux from the body to the brain is boosted. The aim of this study was to investigate if MCT1 expression in hippocampus is upregulated in an animal model of ADHD. We therefore quantified whether there were any differences in MCT1 densities in a rat model of ADHD compared to control. The spontaneously hypertensive rat (SHR) was selected as a model of the disorder because it displays all three main symptoms of ADHD-C, as well as learning difficulties [37, 38]. First, overall MCT1 labelling in hippocampal parenchyma was quantified by the use of immunofluorescence laser scanning microscopy. Second, specific subcellular MCT1 labelling densities on hippocampal abluminal and luminal membranes of microvessel endothelial cells were quantified by the use of postembedding immunogold electron microscopy.

2. MATERIAL AND METHODS

2.1 Animals

Male SHR from Charles River, Germany (SHR/NCrl) was used as a rat model of ADHD and male Wistar Kyoto rat (WKY) from Harlan Europe, UK (WKY/NHsd) served as control. The animals were treated in line with regional and national regulations of animal experiments, and the Norwegian Animal Research Authority approved the experiments performed in this study.

© 2018. This manuscript version is made available under the CC-BY-NC-ND 4.0 license
http://creativecommons.org/licenses/by-nc-nd/4.0/

2.2 Tissue fixation

At postnatal day (PND) 28 WKY (n=12) and SHR (n=12) were anesthetized using 0.3 ml Equithesin per 100 g. The brains were fixed by transcardiac perfusion for 10 min with 4 % paraformaldehyde in 0.1 M phosphate buffer and stored at 4°C in fixation solution. The fixative contained 0.1 % glutaraldehyde in order to conserve the brain ultrastructure in tissue prepared for postembedding immunogold electron microscopy experiments.

2.3 Immunofluorescence laser scanning microscopy

The immunofluorescence laser scanning microscopy procedure was followed as previously described [32, 39]. The brain sections from WKY (n=7) and SHR (n=7) were then treated with rabbit MCT1 primary antibody (AB 1286, Millipore; 1:700) and then with Alexa Fluor 488 goat anti-rabbit-secondary antibody (Invitrogen, Molecular Probes, USA; 1:1000). The negative control was treated equally, except it was not incubated with primary antibody. Micrographs were acquired from neuropil layers of hippocampus (CA1 strata oriens and radiatum and adjacent hilus of the dentate gyrus (in accordance with accurate coordinates and anatomical information from a rat brain atlas [40]) using a confocal laser scanning microscope (Zeiss, Germany). Nine z-stack scans (each consisting of eight images) were acquired from each animal. The micrographs were analysed in the computer program LSM Image Explorer (Zeiss, Germany) and the MCT1 immunoreactivity was calculated by quantifying the amount of pixels multiplied with the fluorescence intensity.

© 2018. This manuscript version is made available under the CC-BY-NC-ND 4.0 license
http://creativecommons.org/licenses/by-nc-nd/4.0/

2.4 Postembedding immunogold electron microscopy

The postembedding immunogold electron microscopy protocol was performed as in previous experiments [32, 39, 41]. Ultrathin sections of Lowicryl embedded tissue blocks (0.5 x 1 x 0.5 mm) from septal/dorsal hippocampus (CA1 and adjacent dentate gyrus subregion) were treated with MCT1 primary antibody (AB 1286, Millipore; 1:700). The tissue was then incubated with goat anti-rabbit secondary antibody (IgG; British Biocell International, UK; 1:20). Micrographs of abluminal and luminal endothelial cell membranes of hippocampal BBB capillaries were acquired in a transmission electron microscope (Tecnai 12; FEI Company, USA; 43 000x primary magnification). The immunoreactivity was quantified with Image J and the plugin "Dist to path" [32]. Gold particles located along luminal and abluminal membrane of microvessel endothelial cells, up to 25 nm on the intracellular or extracellular side of the membrane were recorded as membrane associated [42]. The number of membrane segments observed is taken as the number of observations. The gold particle density on membrane segments were compared between WKY (n=5) and SHR (n=5) from abluminal membranes (119 and 133 segments from WKY and SHR, respectively) and from luminal membranes (144 segments from WKY and 167 segments from SHR).

2.5 Statistical method

As compared to the commonly used two-sample t-test for difference in means, the statistical method applied in this article (see below) has several advantages. Firstly, it allows for investigation of layer-specific differences between WKY and SHR in one comprehensive analysis. We do not have to run separate analyses of luminal and abluminal membranes, but can use the whole data set for each sub-analysis. In other words, we use all the information in

© 2018. This manuscript version is made available under the CC-BY-NC-ND 4.0 license
http://creativecommons.org/licenses/by-nc-nd/4.0/

the total available data in every sub-analysis. Secondly, this method provides an overall estimate of the difference between SHR and WKY that takes account of possible membrane-specific differences. Thirdly, we use a statistical method fit for analysing count data, thereby providing more accurate estimates than the more commonly used linear methods.

We estimate the following regression equations in, respectively, the immunofluorescence laser scanning microscopy experiments and the postembedding immunogold electron microscopy experiments:

(1) $y_{di} = a + b group + e_{di}$

(2) $y_{di} = \alpha + \beta^{g} group + \beta^{l} layer + \beta^{gl} group * layer + \varepsilon_{di}$

where y_{di} is the number of particles in observation *i* from animal *d*. *group* is a categorical variable equal to 0 for WKY and 1 for SHR. b and β^{g} reflect the effects from changing *group* from WKY to SHR in the immunofluorescence laser scanning microscopy and the postembedding immunogold electron microscopy studies, respectively. In the postembedding immunogold electron microscopy study we also include a categorical variable, *layer*, equal to 0 if layer is abluminal and 1 if it is luminal. β^{l} shows the effect of changing *layer* from abluminal to luminal. In addition, we include an interaction effect between *group* and *layer*, β^{gl}. This allows for investigation of whether the *group*-effect differs between layers (and the *layer*-effect differs between groups). Since the dependent variables are count variables, we estimate eq. (1) and (2) using a Poisson regression model. We compute robust standard errors to take into consideration heteroscedasticity arising from, e.g., individual differences between animals.

© 2018. This manuscript version is made available under the CC-BY-NC-ND 4.0 license
http://creativecommons.org/licenses/by-nc-nd/4.0/

We run the regression on the data from the two undertaken studies using the software StataCorp (2017) [43]. To ease the interpretation of the results, we do not present regression coefficients (available on request), but rather the estimated percent changes in y_{di} when the categorical variable of interest changes from the base value (henceforth; $\%\Delta\hat{y}_{di}$). This is calculated with basis in the average marginal effect (AME) in the semi-elasticity form, calculated by the Stata postestimation command *margins, eydx*. In both studies, we present the overall effect of changing group from WKY to SHR[1]. In the postembedding immunogold electron microscopy study we also present the $\%\Delta\hat{y}_{di}$s for all combinations of *group* and *layer*[2]. See the StataCorp manual (2017) [43] and Williams (2012) [44] for a discussion of different types of marginal effects in Stata. When presenting the $\%\Delta\hat{y}_{di}$s, we also report the p-value of the corresponding marginal effect to indicate the statistical significance.

3. RESULTS

3.1 Immunofluorescence laser scanning microscopy

In order to examine overall neuropil MCT1 staining, immunofluorescence laser scanning microscopy was performed. The immunofluorescence staining was particularly strong on distinct round structures corresponding to the size and shape of cross-sectioned microvessels, whereas immunoreactivity in the intervening neuropil was modest (Figure 1). Descriptive statistics are presented in Table 1. The estimated effect from the Poisson regression indicates that the labelling density was 7.61 % higher in SHR as compared to WKY ($p<0.01$).

3.2 Postembedding immunogold electron microscopy

© 2018. This manuscript version is made available under the CC-BY-NC-ND 4.0 license
http://creativecommons.org/licenses/by-nc-nd/4.0/

To assess whether there were any specific differences in MCT1 density on hippocampal microvessels between WKY and SHR, postembedding immunogold electron microscopy was used (Figure 2). The immunogold particles were predominantly present on capillary endothelial cells compared to general neuropil. Luminal and abluminal membranes were especially immunoreactive, only a few particles were observed intracellularly. Labelling densities on luminal and abluminal membranes were quantified separately. See Table 2 for descriptive statistics. The results from the Poisson estimation are presented in Table 3. These indicate significantly higher labelling density in both abluminal and luminal membranes of SHR compared to WKY ($p<0.01$). The overall estimated effect indicates that the level of MCT1 was more than doubled in SHR as compared to WKY (an increase of 140%). More specifically, the estimated increase was 94.7 % and 212 % in abluminal and luminal membranes, respectively. In essence, these estimates indicate that the labelling density in SHR compared to WKY was almost doubled in abluminal and more than tripled in luminal membrane.[3] *Within* WKY, the estimated effect was significantly higher on luminal, compared to abluminal membrane. However, this layer specific difference was not statistically significant within SHR.

4. DISCUSSION

4.1 MCT1 immunoreactivity in CA1 hippocampus

In the current study, immunofluorescence laser scanning confocal microscopy was first used to quantify general MCT1 staining in neuropil layers of hippocampus. Previous studies have demonstrated ubiquitous expression of MCT1 in brain parenchyma, including neurons [16, 19, 45], astrocytes [17, 46] and oligodendrocytes [47, 48]. In line with previous experiments

© 2018. This manuscript version is made available under the CC-BY-NC-ND 4.0 license
http://creativecommons.org/licenses/by-nc-nd/4.0/

[16, 20], the MCT1 immunofluorescence staining was high on capillaries, whereas staining in the intervening neuropil was sparser. The laser scanning microscope has a large field of view which made it possible to effectively investigate quite large areas. However, the spatial resolution of 200 nm did not allow determination of staining to specific cell structures. Therefore, postembedding immunogold electron microscopy, which has a lateral resolution of 25 nm [42], was used to quantify the MCT1 immunolabelling densities on luminal and abluminal plasma membranes of capillary endothelial cells. Furthermore, in the postembedding protocol, only antigens on the surface of the section are available for antibody binding. There is an approximately linear relation between antigen availability and binding of primary and secondary antibodies, which ensures an even potential for antibody binding within and between different brain sections. Hence, postembedding immunogold electron microscopy is considered a precise method both for comparing protein labelling densities on brain sections and for determining protein subcellular localization [49]. The sampling area was however limited, compared to the area examined under immunofluorescence laser scanning microscopy. In congruence with the study by Leino et al. (1999) [16], gold particles were highly present on the membrane compared to intracellularly. These membrane associated immunogold particles are likely functional MCT1s at the BBB, responsible for the lactate flux between body and brain. In our experiments, the labelling density within WKY was lower on abluminal compared to luminal membrane, whereas such a layer specific difference was not statistically significant in SHR. The BBB endothelial cells face different milieus on their luminal and abluminal sides, and the lipid constitutes and the distributions of several BBB transporters vary between luminal and abluminal membranes [50]. Leino and colleges found the MCT1 labelling to be similar on the two kinds of membranes in control rats [16, 51], but under hyperlactemic conditions the MCT1 expression on BBB increased substantially, and the expression pattern was polarized: Suckling rats had 5 % more MCT1

© 2018. This manuscript version is made available under the CC-BY-NC-ND 4.0 license
http://creativecommons.org/licenses/by-nc-nd/4.0/

labelling on abluminal compared to luminal membranes, and rats exposed to ketogenic diet had twice as many MCT1s on the abluminal compared to the luminal membrane [51]. Hence, a polarized MCT1 expression in rats seems to vary with strain, age and condition. However, little is known of the molecular mechanisms underlying BBB polarity [52].

4.2 High MCT1 labelling density in SHR

We demonstrated significantly higher MCT1 immunoreactivity in SHR compared to WKY. Overall staining and specific endothelial staining (quantified by immunofluorescence and electron microscopy, respectively) were both higher in SHR compared to WKY, with the change being highly significant on BBB endothelial cell membranes. The especially high increase in labelling intensity on BBB endothelial cells was probably masked in the immunofluorescence study due to the examination of whole neuropil in the laser scanning microscope compared to the more specific examination of endothelial subcellular localization in the electron microscope. The MCT1 immunoreactivity was significantly higher both on luminal and abluminal membranes of capillaries.

Previous studies have demonstrated that rats are able to upregulate brain MCT1 expression in response to hyperlactatemia. Postnatally, lactate present in breast milk is a main energy source for the developing brain. Leino et al. (1999) showed that suckling rats have 25 times more MCT1 immunogold particles on BBB microvessels compared to adults [16]. In addition, general neuropil MCT1 immunostaining was higher. Similarly to our study, the increase in MCT1 labelling was most prominent at BBB as compared to parenchyma. Also in adulthood, periods of high fat (ketogenic) diet [51] chronic hyperglycemia [53] and exercise [54] are

© 2018. This manuscript version is made available under the CC-BY-NC-ND 4.0 license
http://creativecommons.org/licenses/by-nc-nd/4.0/

followed by an upregulation of MCT1. Interestingly, children with ADHD-C have slightly elevated lactate in their venous blood [55], which may be followed by an increased expression of MCT1, as observed in this study. Psychosocial stress raises the level of plasma adrenalin and plasma lactate, possibly to meet the high energy demand of the brain during stressful situations [56]. Interestingly, physical stress such as exercise, raises the level of lactate significantly more in children with ADHD than in controls, but with only a modest increase in the catecholamine concentration in the ADHD group compared to controls [57]. Consequently, dysfunctional catecholamine stimulation does not seem to blunt peripheral lactate production as may be the case for lactate production in the brain [7]. As already described, brain astrocytes produce lactate, and the direction of flux between the body and the brain depend on concentration gradient. Hence, to verify the role of lactate and lactate transporters, functional studies of lactate flux and concentrations in the blood and brain would be optimal.

Recent data suggest that lactate produced during exercise activates a brain lactate receptor (hydroxycarboxylic acid receptor 1- also called G-protein coupled receptor 81) which in turn increases levels of growth factors important to angiogenesis, neurogenesis and synaptic plasticity [58]. Hence, lactate entering the brain through MCT1s may serve both as an energy source and as a signalling molecule in the brain. In addition, brain astrocytes, neurons and oligodendrocytes utilize lactate as a precursor for lipids [59]. Interestingly, the subgranular zone of the dentate gyrus in hippocampus is one of two brain regions in which new neurons are generated throughout adult life [60, 61]. Structural brain changes, such as a reduction in myelin caused by low lactate availability for oligodendrocytes [48], could affect overall neuronal signaling and result in symptoms of ADHD [14]. In fact, children with ADHD show

© 2018. This manuscript version is made available under the CC-BY-NC-ND 4.0 license
http://creativecommons.org/licenses/by-nc-nd/4.0/

abnormal myelination in the brain [62]. They also have smaller hippocampal volume [28, 63] and disrupted network connectivity between hippocampus and orbitofrontal cortex [28]. Hence, low brain lactate may cause both short- and long-term structural and functional changes observed in ADHD. ADHD is categorized as a neurodevelopmental disorder, with the exact onset being debated [2]. Importantly, the function of lactate and MCT1 is significant both to the developing and adult brain.

4.3 Is hyperactivity a form of self-treatment in ADHD?

SHR/NCrl systematically display hyperactive, inattentive and impulsive behaviour compared to WKY/NHsd, its optimal control [37, 38, 64-67]. Previous studies have shown that physical exercise reduces symptoms of hyperactivity [68, 69] impulsivity [68, 70, 71] and inattention in SHR [72] Most research performed in humans with ADHD acknowledges exercise to have a positive effect on behaviour and executive function [73, 74]. Hyperactivity is considered a core symptom of ADHD including various forms of excess motor activity in non-suitable situations [2]. Controversially, hyperactivity has been considered a compensatory mechanism in ADHD; increased motor activity seems to improve cognitive performance in children with ADHD [36], and the hyperactive behaviour is more frequent in situations that acquire high executive brain function [35]. Excess gross motor activity observed in children with ADHD, may enhance skeletal muscle lactate production and lead to higher levels of MCT1 at the BBB, as observed in SHR in our experiments. The increased level of MCT1s at the BBB could have a positive effect in SHR, bringing more peripheral lactate into the brain if its intrinsic lactate concentration is low. In this study we explored the level of MCT1 in WKY and SHR to elucidate a possible link between hyperactivity and brain function in ADHD. MCT1 expressed at the BBB is the only lactate transporter that may shuttle plasma lactate into

© 2018. This manuscript version is made available under the CC-BY-NC-ND 4.0 license
http://creativecommons.org/licenses/by-nc-nd/4.0/

the brain in response to increased motor activity. To further explore the role of lactate transport within the brain in ADHD, it would be interesting to follow up with quantitative studies of MCT2 and MCT4 levels on neurons and astrocytes in WKY and SHR. Furthermore, it would be interesting to investigate both expression and function of the newly discovered brain lactate receptor GPR81, in these rats.

In the current study, we used the subtype SHR/NCrl that is validated as the best animal model of ADHD-C and WKY/NHsd that is evaluated as the best matched control [37, 38]. The use of brain sections from these rats allowed us to determine MCT1 labelling density in specific subcellular compartments, which is not possible to study in humans. However, the development of appropriate animal models for studying human psychiatric disorders like ADHD is a challenge [75], due to lack of biological markers and heterogeneous appearance of the disorder. Despite this, SHRs used in this study and children with ADHD display comparable genetics, development, behavior and response to medications [37, 38]. However, the development of other diseases, such as hypertension in SHR may be a confounding factor. To minimize this problem in our experiments, rats were sacrificed at PND28 at an age in which SHR display symptoms similar as children with ADHD, and before hypertension develop. In our study, we used only male WKYs and SHRs, in order to minimize variability and in agreement with the common notion that ADHD prevalence is highest among males. While the use of males only is a limitation of the study with respect to relevance for which may limit the impact of the results on female ADHD symptomatology, only small gender differences have been found in the characteristics of ADHD [76]. Based on the current stage of knowledge, we support that hyperactivity in ADHD may be a form of self-treatment. We are well aware of that further studies both in humans and in animal models of ADHD are

© 2018. This manuscript version is made available under the CC-BY-NC-ND 4.0 license
http://creativecommons.org/licenses/by-nc-nd/4.0/

necessary to verify the effects of physical activity on core symptoms of the disorder and to identify corresponding mechanisms at microscopic levels in the brain. Active skeletal muscles produce several metabolites in addition to lactate that may affect brain function [77]. With further understanding of basic mechanisms, alternative treatment strategies like physical activity may be a part of future ADHD therapy for humans.

CONFLICT OF INTEREST

There are no conflicts of interest.

FUNDING

This work was supported by the Norwegian National Research Network for ADHD and the Research Council of Norway (RCN).

ACKNOWLEDGMENTS

We would like to thank Øyvind Skare for advice on statistics.

REFERENCES

© 2018. This manuscript version is made available under the CC-BY-NC-ND 4.0 license
http://creativecommons.org/licenses/by-nc-nd/4.0/

1. Polanczyk, G.V., et al., *ADHD prevalence estimates across three decades: an updated systematic review and meta-regression analysis.* Int J Epidemiol, 2014. **43**(2): p. 434-42.
2. Association, A.P., *Diagnostic and Statistical Manual of Mental Disorders*. 5th ed. ed. 2013:

Washington, DC: American Psychiatric Publishing.

3. Thapar, A., et al., *What have we learnt about the causes of ADHD?* J Child Psychol Psychiatry, 2013. **54**(1): p. 3-16.
4. Tripp, G. and J.R. Wickens, *Neurobiology of ADHD.* Neuropharmacology, 2009. **57**(7-8): p. 579-89.
5. Killeen, P.R., V.A. Russell, and J.A. Sergeant, *A behavioral neuroenergetics theory of ADHD.* Neurosci Biobehav Rev, 2013. **37**(4): p. 625-57.
6. Russell, V.A., et al., *Response variability in Attention-Deficit/Hyperactivity Disorder: a neuronal and glial energetics hypothesis.* Behav Brain Funct, 2006. **2**: p. 30.
7. Todd, R.D. and K.N. Botteron, *Is attention-deficit/hyperactivity disorder an energy deficiency syndrome?* Biol Psychiatry, 2001. **50**(3): p. 151-8.
8. Attwell, D. and S.B. Laughlin, *An energy budget for signaling in the grey matter of the brain.* J Cereb Blood Flow Metab, 2001. **21**(10): p. 1133-45.
9. Schurr, A., C.A. West, and B.M. Rigor, *Lactate-supported synaptic function in the rat hippocampal slice preparation.* Science, 1988. **240**(4857): p. 1326-8.
10. van Hall, G., et al., *Blood lactate is an important energy source for the human brain.* J Cereb Blood Flow Metab, 2009. **29**(6): p. 1121-9.
11. Dringen, R., R. Gebhardt, and B. Hamprecht, *Glycogen in astrocytes: possible function as lactate supply for neighboring cells.* Brain Res, 1993. **623**(2): p. 208-14.
12. Pellerin, L., et al., *Evidence supporting the existence of an activity-dependent astrocyte-neuron lactate shuttle.* Dev Neurosci, 1998. **20**(4-5): p. 291-9.
13. Suzuki, A., et al., *Astrocyte-neuron lactate transport is required for long-term memory formation.* Cell, 2011. **144**(5): p. 810-23.
14. Sagvolden, T., et al., *A dynamic developmental theory of attention-deficit/hyperactivity disorder (ADHD) predominantly hyperactive/impulsive and combined subtypes.* Behav. Brain Sci, 2005. **28**(3): p. 397-419.

© 2018. This manuscript version is made available under the CC-BY-NC-ND 4.0 license
http://creativecommons.org/licenses/by-nc-nd/4.0/

15. Halestrap, A.P. and N.T. Price, *The proton-linked monocarboxylate transporter (MCT) family: structure, function and regulation.* Biochem J, 1999. **343 Pt 2**: p. 281-99.
16. Leino, R.L., D.Z. Gerhart, and L.R. Drewes, *Monocarboxylate transporter (MCT1) abundance in brains of suckling and adult rats: a quantitative electron microscopic immunogold study.* Brain Res Dev Brain Res, 1999. **113**(1-2): p. 47-54.
17. Pierre, K., et al., *Cell-specific localization of monocarboxylate transporters, MCT1 and MCT2, in the adult mouse brain revealed by double immunohistochemical labeling and confocal microscopy.* Neuroscience, 2000. **100**(3): p. 617-27.
18. Bergersen, L., A. Rafiki, and O.P. Ottersen, *Immunogold cytochemistry identifies specialized membrane domains for monocarboxylate transport in the central nervous system.* Neurochem Res, 2002. **27**(1-2): p. 89-96.
19. Pellerin, L., et al., *Cellular and subcellular distribution of monocarboxylate transporters in cultured brain cells and in the adult brain.* J Neurosci Res, 2005. **79**(1-2): p. 55-64.
20. Gerhart, D.Z., et al., *Expression of monocarboxylate transporter MCT1 by brain endothelium and glia in adult and suckling rats.* Am J Physiol, 1997. **273**(1 Pt 1): p. E207-13.
21. Mueller, A., et al., *Linking ADHD to the Neural Circuitry of Attention.* Trends Cogn Sci, 2017. **21**(6): p. 474-488.
22. Emond, V., C. Joyal, and H. Poissant, *[Structural and functional neuroanatomy of attention-deficit hyperactivity disorder (ADHD)]*. Encephale, 2009. **35**(2): p. 107-14.
23. Goodman, J., et al., *Annual research review: The neurobehavioral development of multiple memory systems--implications for childhood and adolescent psychiatric disorders.* J Child Psychol Psychiatry, 2014. **55**(6): p. 582-610.
24. Axmacher, N., et al., *Cross-frequency coupling supports multi-item working memory in the human hippocampus.* Proc Natl Acad Sci U S A, 2010. **107**(7): p. 3228-33.
25. Bliss, T.V. and T. Lomo, *Long-lasting potentiation of synaptic transmission in the dentate area of the anaesthetized rabbit following stimulation of the perforant path.* J Physiol, 1973. **232**(2): p. 331-356.
26. Johansen, E.B., et al., *Attention-deficit/hyperactivity disorder (ADHD) behaviour explained by dysfunctioning reinforcement and extinction processes.* Behav Brain Res, 2002. **130**(1-2): p. 37-45.

© 2018. This manuscript version is made available under the CC-BY-NC-ND 4.0 license
http://creativecommons.org/licenses/by-nc-nd/4.0/

27. Sagvolden, T. and J.A. Sergeant, *Attention deficit/hyperactivity disorder--from brain dysfunctions to behaviour.* Behav Brain Res, 1998. **94**(1): p. 1-10.
28. Posner, J., et al., *A multimodal MRI study of the hippocampus in medication-naive children with ADHD: what connects ADHD and depression?* Psychiatry Res, 2014. **224**(2): p. 112-8.
29. Al-Amin, M., A. Zinchenko, and T. Geyer, *Hippocampal subfield volume changes in subtypes of attention deficit hyperactivity disorder.* Brain Res, 2018. **1685**: p. 1-8.
30. Maurer, M.H., et al., *Correlation between local monocarboxylate transporter 1 (MCT1) and glucose transporter 1 (GLUT1) densities in the adult rat brain.* Neurosci Lett, 2004. **355**(1-2): p. 105-8.
31. Jensen, V., et al., *N-methyl-D-aspartate receptor subunit dysfunction at hippocampal glutamatergic synapses in an animal model of attention-deficit/hyperactivity disorder.* Neuroscience, 2009. **158**(1): p. 353-64.
32. Medin, T., et al., *Low dopamine D5 receptor density in hippocampus in an animal model of attention-deficit/hyperactivity disorder (ADHD).* Neuroscience, 2013. **242**: p. 11-20.
33. Sterley, T.L., F.M. Howells, and V.A. Russell, *Nicotine-stimulated release of [3H]norepinephrine is reduced in the hippocampus of an animal model of attention-deficit/hyperactivity disorder, the spontaneously hypertensive rat.* Brain Res, 2014. **1572**: p. 1-10.
34. Sterley, T.L., F.M. Howells, and V.A. Russell, *Evidence for reduced tonic levels of GABA in the hippocampus of an animal model of ADHD, the spontaneously hypertensive rat.* Brain Res, 2013. **1541**: p. 52-60.
35. Kofler, M.J., et al., *Is hyperactivity ubiquitous in ADHD or dependent on environmental demands? Evidence from meta-analysis.* Clin Psychol Rev, 2016. **46**: p. 12-24.
36. Sarver, D.E., et al., *Hyperactivity in Attention-Deficit/Hyperactivity Disorder (ADHD): Impairing Deficit or Compensatory Behavior?* J Abnorm Child Psychol, 2015. **43**(7): p. 1219-32.
37. Russell, V.A., *Overview of animal models of attention deficit hyperactivity disorder (ADHD).* Curr. Protoc. Neurosci, 2011. **Chapter 9**: p. Unit9.
38. Sagvolden, T. and E.B. Johansen, *Rat models of ADHD.* Curr. Top. Behav. Neurosci, 2012. **9**: p. 301-315.

© 2018. This manuscript version is made available under the CC-BY-NC-ND 4.0 license
http://creativecommons.org/licenses/by-nc-nd/4.0/

39. Medin, T., et al., *Dopamine D5 receptors are localized at asymmetric synapses in the rat hippocampus.* Neuroscience, 2011. **192**: p. 164-171.
40. Paxinos, G.W., Charles, *The Rat Brain in Stereotaxic Coordinates*. 7 ed. 2013, London: Academic Press.
41. Bergersen, L.H., J. Storm-Mathisen, and V. Gundersen, *Immunogold quantification of amino acids and proteins in complex subcellular compartments.* Nat Protoc, 2008. **3**(1): p. 144-52.
42. Ottersen, O.P., *Quantitative electron microscopic immunocytochemistry of neuroactive amino acids.* Anat. Embryol. (Berl), 1989. **180**(1): p. 1-15.
43. StataCorp., *Stata Statistical Software: Release 15. College Station, TX: StataCorp LLC.* 2017.
44. Williams , R., *Using the margins command to estimate and interpret adjusted predictions and marginal effects.* Stata Journal, 2012. **12**(2): p. 308–331
45. Debernardi, R., et al., *Cell-specific expression pattern of monocarboxylate transporters in astrocytes and neurons observed in different mouse brain cortical cell cultures.* J Neurosci Res, 2003. **73**(2): p. 141-55.
46. Broer, S., et al., *Comparison of lactate transport in astroglial cells and monocarboxylate transporter 1 (MCT 1) expressing Xenopus laevis oocytes. Expression of two different monocarboxylate transporters in astroglial cells and neurons.* J Biol Chem, 1997. **272**(48): p. 30096-102.
47. Lee, Y., et al., *Oligodendroglia metabolically support axons and contribute to neurodegeneration.* Nature, 2012. **487**(7408): p. 443-8.
48. Rinholm, J.E., et al., *Regulation of oligodendrocyte development and myelination by glucose and lactate.* J Neurosci, 2011. **31**(2): p. 538-48.
49. Mathiisen, T.M., et al., *Postembedding Immunogold Cytochemistry of Membrane Molecules and Amino Acid Transmitters in the Central Nervous System*, in *Neuroanatomical Tract-Tracing 3*, W.F.G. Zaborszky L., Lanciego J.L. (eds), Editor. 2006. p. 72-108.
50. Cornford, E.M. and S. Hyman, *Localization of brain endothelial luminal and abluminal transporters with immunogold electron microscopy.* NeuroRx, 2005. **2**(1): p. 27-43.
51. Leino, R.L., et al., *Diet-induced ketosis increases monocarboxylate transporter (MCT1) levels in rat brain.* Neurochem Int, 2001. **38**(6): p. 519-27.

© 2018. This manuscript version is made available under the CC-BY-NC-ND 4.0 license
http://creativecommons.org/licenses/by-nc-nd/4.0/

52. Lampugnani, M.G., et al., *CCM1 regulates vascular-lumen organization by inducing endothelial polarity.* J Cell Sci, 2010. **123**(Pt 7): p. 1073-80.
53. Canis, M., et al., *Increased densities of monocarboxylate transporter MCT1 after chronic hyperglycemia in rat brain.* Brain Res, 2009. **1257**: p. 32-9.
54. Takimoto, M. and T. Hamada, *Acute exercise increases brain region-specific expression of MCT1, MCT2, MCT4, GLUT1, and COX IV proteins.* J Appl Physiol (1985), 2014. **116**(9): p. 1238-50.
55. Hasan, C.M., et al., *Prevalence and assessment of biochemical parameters of attention-deficit hyperactivity disorder children in Bangladesh.* J Basic Clin Pharm, 2016. **7**(3): p. 70-4.
56. Kubera, B., et al., *Rise in plasma lactate concentrations with psychosocial stress: a possible sign of cerebral energy demand.* Obes Facts, 2012. **5**(3): p. 384-92.
57. Wigal, S.B., et al., *Catecholamine response to exercise in children with attention deficit hyperactivity disorder.* Pediatr Res, 2003. **53**(5): p. 756-61.
58. Morland, C., et al., *Exercise induces cerebral VEGF and angiogenesis via the lactate receptor HCAR1.* Nat Commun, 2017. **8**: p. 15557.
59. Medina, J.M. and A. Tabernero, *Lactate utilization by brain cells and its role in CNS development.* J Neurosci Res, 2005. **79**(1-2): p. 2-10.
60. Zhao, C., W. Deng, and F.H. Gage, *Mechanisms and functional implications of adult neurogenesis.* Cell, 2008. **132**(4): p. 645-60.
61. Kaplan, M.S. and J.W. Hinds, *Neurogenesis in the adult rat: electron microscopic analysis of light radioautographs.* Science, 1977. **197**(4308): p. 1092-4.
62. Nagel, B.J., et al., *Altered white matter microstructure in children with attention-deficit/hyperactivity disorder.* J Am Acad Child Adolesc Psychiatry, 2011. **50**(3): p. 283-92.
63. Hoogman, M., et al., *Subcortical brain volume differences in participants with attention deficit hyperactivity disorder in children and adults: a cross-sectional mega-analysis.* Lancet Psychiatry, 2017. **4**(4): p. 310-319.
64. Dervola, K.S., et al., *Marine omega-3 polyunsaturated fatty acids induce sex-specific changes in reinforcer-controlled behaviour and neurotransmitter metabolism in a spontaneously hypertensive rat model of ADHD.* Behav. Brain Funct, 2012. **8**(1): p. 56.

© 2018. This manuscript version is made available under the CC-BY-NC-ND 4.0 license
http://creativecommons.org/licenses/by-nc-nd/4.0/

65. Jensen, V., et al., *N-methyl-D-aspartate receptor subunit dysfunction at hippocampal glutamatergic synapses in an animal model of attention-deficit/hyperactivity disorder.* Neuroscience, 2009. **158**(1): p. 353-364.
66. Sagvolden, T., et al., *Behavioral and genetic evidence for a novel animal model of Attention-Deficit/Hyperactivity Disorder Predominantly Inattentive Subtype.* Behav. Brain Funct, 2008. **4**: p. 56.
67. Sagvolden, T., et al., *The spontaneously hypertensive rat model of ADHD--the importance of selecting the appropriate reference strain.* Neuropharmacology, 2009. **57**(7-8): p. 619-626.
68. Cho, H.S., D.J. Baek, and S.S. Baek, *Effect of exercise on hyperactivity, impulsivity and dopamine D2 receptor expression in the substantia nigra and striatum of spontaneous hypertensive rats.* J Exerc Nutrition Biochem, 2014. **18**(4): p. 379-84.
69. Ji, E.S., et al., *Duration-dependence of the effect of treadmill exercise on hyperactivity in attention deficit hyperactivity disorder rats.* J Exerc Rehabil, 2014. **10**(2): p. 75-80.
70. Robinson, A.M. and D.J. Bucci, *Individual and combined effects of physical exercise and methylphenidate on orienting behavior and social interaction in spontaneously hypertensive rats.* Behav Neurosci, 2014. **128**(6): p. 703-12.
71. Baek, D.J., C.B. Lee, and S.S. Baek, *Effect of treadmill exercise on social interaction and tyrosine hydroxylase expression in the attention-deficit/ hyperactivity disorder rats.* J Exerc Rehabil, 2014. **10**(5): p. 252-7.
72. Robinson, A.M., M.E. Hopkins, and D.J. Bucci, *Effects of physical exercise on ADHD-like behavior in male and female adolescent spontaneously hypertensive rats.* Dev Psychobiol, 2011. **53**(4): p. 383-90.
73. Cerrillo-Urbina, A.J., et al., *The effects of physical exercise in children with attention deficit hyperactivity disorder: a systematic review and meta-analysis of randomized control trials.* Child Care Health Dev, 2015. **41**(6): p. 779-88.
74. Den Heijer, A.E., et al., *Sweat it out? The effects of physical exercise on cognition and behavior in children and adults with ADHD: a systematic literature review.* J Neural Transm (Vienna), 2017. **124**(Suppl 1): p. 3-26.
75. Nestler, E.J. and S.E. Hyman, *Animal models of neuropsychiatric disorders.* Nat Neurosci, 2010. **13**(10): p. 1161-9.
76. Rucklidge, J.J., *Gender differences in attention-deficit/hyperactivity disorder.* Psychiatr Clin North Am, 2010. **33**(2): p. 357-73.

© 2018. This manuscript version is made available under the CC-BY-NC-ND 4.0 license
http://creativecommons.org/licenses/by-nc-nd/4.0/

77. Delezie, J. and C. Handschin, *Endocrine Crosstalk Between Skeletal Muscle and the Brain.* Front Neurol, 2018. **9**: p. 698.
78. Wooldridge, J.M., *Introductory Econometrics: A Modern Approach*. 2 ed, ed. O. Mason. 2003: Thomson South-Western.

TABLES WITH HEADING AND LEGEND

Table 1. Counts per area in the immunofluorescence laser scanning microscopy study

WKY					**SHR**				
# obs	**Mean**	**Std. dev.**	**Min Value**	**Max Value**	**# obs**	**Mean**	**Std. dev.**	**Min Value**	**Max Value**
378	7252	2373	1375	13508	353	7952	3142	2118	17378

© 2018. This manuscript version is made available under the CC-BY-NC-ND 4.0 license
http://creativecommons.org/licenses/by-nc-nd/4.0/

Table 1. Summary of the number of observations (# obs), mean, standard deviation (std. dev.), minimum (min) and maximum (max) value in Wistar Kyoto rat (WKY) (left) and spontaneously hypertensive rat (SHR) (right)

Table 2. Counts per area in the postembedding immunogold electron microscopy study

	WKY					**SHR**				
	# obs	**Mean**	**Std. dev.**	**Min Value**	**Max Value**	**# obs**	**Mean**	**Std. dev.**	**Min Value**	**Max Value**
Whole sample	263	8.107	11.23	0.000	61.47	300	18.69	16.80	0.000	74.22
Abluminal	119	6.548	11.01	0.000	59.12	133	19.82	18.04	0.000	74.22

© 2018. This manuscript version is made available under the CC-BY-NC-ND 4.0 license
http://creativecommons.org/licenses/by-nc-nd/4.0/

Luminal	144	9.396	11.30	0.000	61.47	167	17.79	15.74	0.000	70.01

Table 2. This table shows the number of observations (# obs), mean, standard deviation (std. dev.), minimum (min) and maximum (max) value in whole sample, abluminal and luminal membranes in Wistar Kyoto rat (WKY) (left) and spontaneously hypertensive rat (SHR) (right).

Table 3. Estimated per cent changes in the number of immunogold particles

Effect of changing	**For**	**Estimated % change***	**p-value marginal effect****
***group* from WKY to SHR**	**Overall**	140	0.000
	***layer* = abluminal**	212	0.000
	***layer* = luminal**	94.7	0.000
***layer* from abluminal to**	***group* = WKY**	42.8	0.046

© 2018. This manuscript version is made available under the CC-BY-NC-ND 4.0 license
http://creativecommons.org/licenses/by-nc-nd/4.0/

luminal	***group* = SHR**	-10.8	0.273

Note: Results from Poisson regression estimations of the number of particles in a segment. Robust standard errors. *Calculated with basis in the average marginal effect. **The marginal effects are calculated using the StataCorp (2017) postestimation command margins, eydx()[43]

Table 3. The estimated percent changes between abluminal and luminal layers between Wistar Kyoto rat (WKY) and spontaneously hypertensive rat (SHR) (row 1) and within WKY and SHR (row 2).

HEADING AND LEGEND TO FIGURES

Figure 1 Immunofluorescence labelling

The micrographs show immunofluorescence labelling against MCT1 (green) from WKY (a) and SHR (b). Strong staining is present on round structures probably representing brain capillaries. Some week fluorescence is visible in the rest of the neuropil. Scale bar=10 µm.

© 2018. This manuscript version is made available under the CC-BY-NC-ND 4.0 license
http://creativecommons.org/licenses/by-nc-nd/4.0/

The immunofluorescence labelling was significantly higher in SHR compared to WKY p=0.01 (see table 1 for statistics).

Figure 2 Immunogold labelling

Micrographs from WKY (a) and SHR (b) showing immunogold labelling against MCT1 on capillary endothelial cells. The gold particles are present on abluminal and luminal endothelial cell membranes. The immunogold particles are indicated with red arrows. Scale bar=100 nm. There was significantly higher labelling density in SHR compared to WKY on both abluminal and luminal membranes (see table 2 and 3 for statistics). endo=endothelial cells, lum=lumen of capillary.

FOOTNOTES

[1]The AME in the semi-elasticity form is equal to the average of the changes in the predicted $\ln(y_{di}s)$ when *group* changes from WKY to SHR (setting *layer* equal to the observed values in the electron microscopy study study). A small AME in the semi-elasticity form is very similar

© 2018. This manuscript version is made available under the CC-BY-NC-ND 4.0 license
http://creativecommons.org/licenses/by-nc-nd/4.0/

to $\%\Delta\hat{y}_{di}$, but for a large value we must use the following formula to find the correct estimated per cent change: $\%\Delta\hat{y}_{di} = 100*(\exp AME-1)$ [78].

[2]These correspond to the marginal effects at representative values (MERs) and are calculated using the following formulas: for *group* = WKY, $\%\Delta\hat{y}_{di} = 100*(\exp(\beta^{g}-1)$; for *layer* = abluminal, $\%\Delta\hat{y}_{di} = 100*(\exp(\beta^{l}-1)$; for *group* = SHR, $\%\Delta\hat{y}_{di} = 100*(\exp(\beta^{g}+\beta^{gl})-1)$; and for *layer* = luminal, $\%\Delta\hat{y}_{di} = 100*(\exp(\beta^{l}+\beta^{gl})-1)$.

[3]The effect is also significantly larger in abluminal; the regression results yield a significantly negative estimated β^{gl} from eq. (2) ($p<0.05$).

© 2018. This manuscript version is made available under the CC-BY-NC-ND 4.0 license
http://creativecommons.org/licenses/by-nc-nd/4.0/

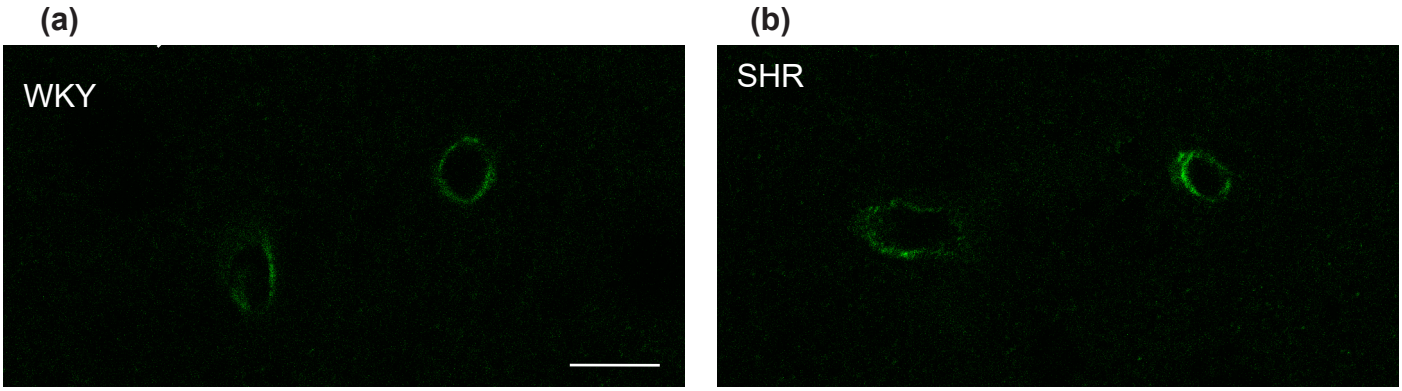

© 2018. This manuscript version is made available under the CC-BY-NC-ND 4.0 license
http://creativecommons.org/licenses/by-nc-nd/4.0/

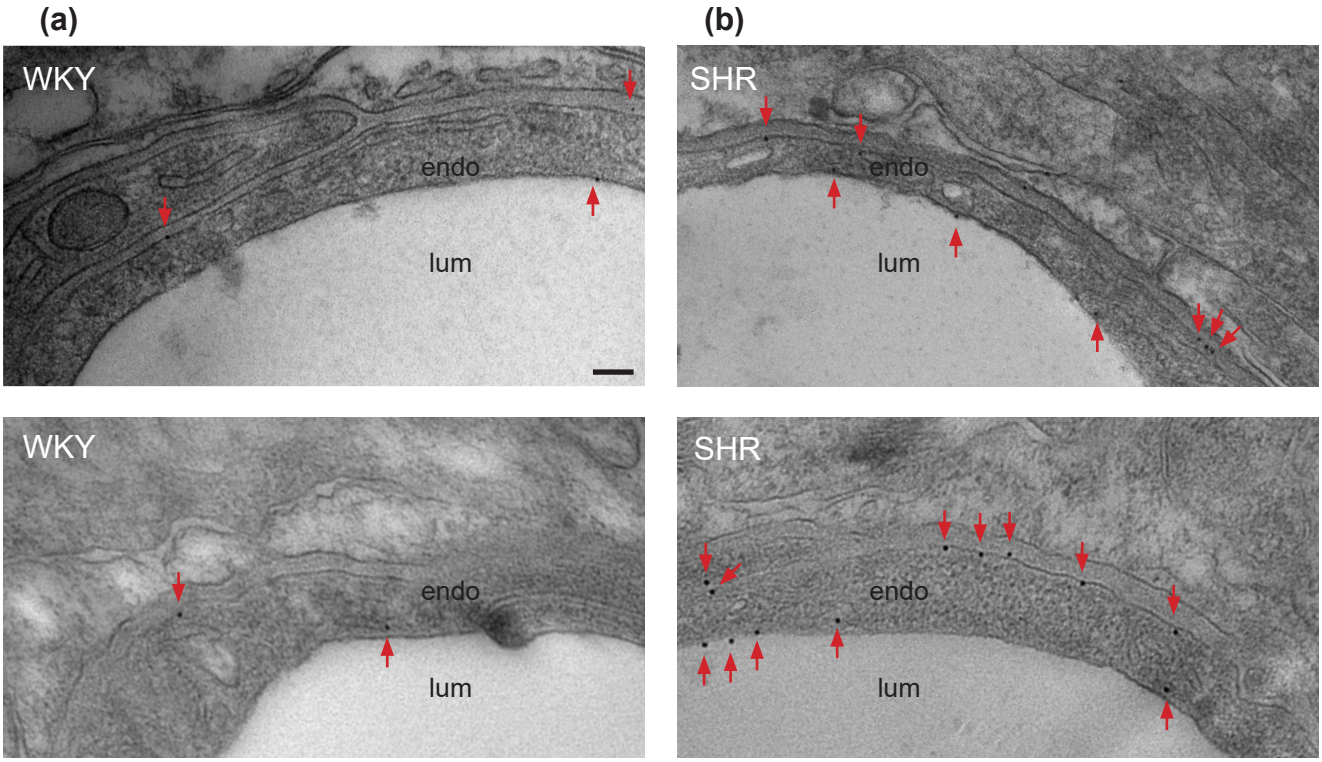

© 2018. This manuscript version is made available under the CC-BY-NC-ND 4.0 license
http://creativecommons.org/licenses/by-nc-nd/4.0/